Since January 2020 Elsevier has created a COVID-19 resource centre with free information in English and Mandarin on the novel coronavirus COVID-19. The COVID-19 resource centre is hosted on Elsevier Connect, the company's public news and information website.

Elsevier hereby grants permission to make all its COVID-19-related research that is available on the COVID-19 resource centre - including this research content - immediately available in PubMed Central and other publicly funded repositories, such as the WHO COVID database with rights for unrestricted research re-use and analyses in any form or by any means with acknowledgement of the original source. These permissions are granted for free by Elsevier for as long as the COVID-19 resource centre remains active.

Water Research 200 (2021) 117243

Contents lists available at ScienceDirect

Water Research

journal homepage: www.elsevier.com/locate/watres

Ultra-fast and onsite interrogation of Severe Acute Respiratory Syndrome Coronavirus 2 (SARS-CoV-2) in waters via surface enhanced Raman scattering (SERS)

Dayi Zhang[a,*], Xiaoling Zhang[b], Rui Ma[b,c], Songqiang Deng[b,c], Xinzi Wang[a], Xinquan Wang[d], Xian Zhang[a], Xia Huang[a], Yi Liu[a], Guanghe Li[a], Jiuhui Qu[a,e], Yu Zhu[f], Junyi Li[b,**]

[a] School of Environment, Tsinghua University, Beijing 100084, P.R. China
[b] Suzhou Yiqing Environmental Science and Technology LTD., Suzhou 215163, P.R. China
[c] Research Institute for Environmental Innovation (Tsinghua-Suzhou), Suzhou 215163, P.R. China
[d] School of Life Science, Tsinghua University, Beijing 100084, P.R. China
[e] Key Laboratory of Drinking Water Science and Technology, Research Center for Eco-Environmental Sciences, Chinese Academy of Sciences, Beijing 100085, P.R. China
[f] Suzhou Institute of Nano-Tech and Nano-Bionics, Chinese Academy of Sciences, 398 Ruoshui Road, Suzhou Industrial Park, Suzhou 215123, P.R. China

ARTICLE INFO

Article history:
Received 29 October 2020
Revised 26 March 2021
Accepted 8 May 2021
Available online 13 May 2021

Keywords:
SARS-CoV-2
Surface enhanced Raman scattering (SERS)
Human receptor angiotensin converting enzyme 2 (ACE2)
Wastewater-based epidemiology

ABSTRACT

The outbreak of coronavirus infectious disease-2019 (COVID-19) pneumonia challenges the rapid interrogation of the severe acute respiratory syndrome coronavirus 2 (SARS-CoV-2) in human and environmental samples. In this study, we developed an assay using surface enhanced Raman scattering (SERS) coupled with multivariate analysis to detect SARS-CoV-2 in an ultra-fast manner without any pretreatment (e.g., RNA extraction). Using silver-nanorod SERS array functionalized with cellular receptor angiotensin-converting enzyme 2 (ACE2), we obtained strong SERS signals of ACE2 at 1032, 1051, 1089, 1189, 1447 and 1527 cm^{-1}. The recognition and binding of receptor binding domain (RBD) of SARS-CoV-2 spike protein on SERS assay significantly quenched the spectral intensities of most peaks and exhibited a shift from 1189 to 1182 cm^{-1}. On-site tests on 23 water samples with a portable Raman spectrometer proved its accuracy and easy-operation for spot detection of SARS-CoV-2 to evaluate disinfection performance, explore viral survival in environmental media, assess viral decay in wastewater treatment plant and track SARS-CoV-2 in pipe network. Our findings raise a state-of-the-art spectroscopic tool to screen and interrogate viruses with RBD for human cell entry, proving its feasibility and potential as an ultra-fast detection tool for wastewater-based epidemiology.

© 2021 Elsevier Ltd. All rights reserved.

1. Introduction

The outbreak of coronavirus infectious disease-2019 (COVID-19) pneumonia since 2019 is caused by the severe acute respiratory syndrome coronavirus 2 (SARS-CoV-2) (Li et al., 2020b) and it has rapidly spread throughout 202 countries around the world. Till 19th March 2021, there have been over 125 million confirmed cases and nearly 3 million deaths globally, and the number is still increasing rapidly. As there is clear evidence of human-to-human transmission of SARS-CoV-2 (Chan et al., 2020; Chang et al., 2020; Li et al., 2020b; Poon and Peiris, 2020), e.g., direct contact, respiratory droplets (Carlos et al., 2020; Lai et al., 2020; Wu et al., 2020) and stools (Zhang et al., 2020b), how to interrogate SARS-CoV-2 in human and environmental samples draws more attentions for effectively confirming COVID-19 cases and identifying transmission routes (Zhang et al., 2021). It brings urgent requirement of developing detection tools that can rapidly and specifically recognize SARS-CoV-2 to track patients.

Many approaches can detect SARS-CoV-2 with high specificity, e.g., real-time reverse transcription quantitative polymerase chain reaction (RT-qPCR) and colloidal gold immunochromatography. RT-qPCR targeted viral specific RNA fragment with specific primers for the open reading frame 1ab (CDDC–ORF), nucleocapsid protein

* Corresponding author at: School of Environment, Tsinghua University, Beijing 100084, P.R. China.
** Corresponding author at: Suzhou Yiqing Environmental Science and Technology LTD., Suzhou 215163, P.R. China.
E-mail addresses: zhangdayi@tsinghua.edu.cn (D. Zhang), junyi_sz@163.com (J. Li).

https://doi.org/10.1016/j.watres.2021.117243
0043-1354/© 2021 Elsevier Ltd. All rights reserved.

(CDDC–N), envelope protein, membrane protein, or RNA-dependent RNA polymerase (RdRp) (Jung et al., 2020; Nalla et al., 2020; Ong et al., 2020; Wang et al., 2020). RNA extraction from swab samples is necessary for RT-qPCR and requires time-consuming pretreatment, normally taking more than 4 h (Nolan et al., 2006; Schmittgen and Livak, 2008) and bringing a barrier for rapid diagnosis of SARS-CoV-2. Alternatively, colloidal gold immunochromatography is a commonly used immunoassay to detect antibodies (IgG or IgM) stimulated by antigen entry (Auta et al., 2017), targeting the immunological markers, IgM and IgG antibodies, which are reported to increase in the blood of most patients more than a week after infection (Woo et al., 2005). However, this method is still time-consuming and not feasible for detecting SARS-CoV-2 in environmental media which do not have immunological markers (Amanat et al., 2020; Stadlbauer et al., 2020; Weiss et al., 2020). It is of great urgency to develop a rapid, reproducible, cheap and sensitive assay detecting SARS-CoV-2, especially applicable for different environmental samples.

Raman spectroscopy is a vibrational spectroscopy of ability to detect chemical bonds via photon scattering (Morais et al., 2019), but the generated signals are extremely weak comparing to the incident beam. Thus, surface enhanced Raman scattering (SERS) is introduced to overcome such inherent limitation and interrogate trace materials by exploiting the enormous electromagnetic field enhancement resulted from the excitation of localized surface plasmon resonances at nanostructured metallic surfaces, mostly gold or silver (Moskovits, 1985; Stiles et al., 2008). It has been widely applied for biological analysis, e.g., living cell classification (Nam et al., 2019), cancer detection (Vendrell et al., 2013), biological imaging (Zavaleta et al., 2009) and virus detection (Zhang et al., 2011). For SARS-CoV-2, the spike glycoprotein consists of S1 and S2 subunits, and S1 subunit contains a receptor binding domain (RBD) directly recognizing the human receptor angiotensin converting enzyme 2 (ACE2) for cell entry (Lan et al., 2020; Zhao et al., 2020). Such recognition and binding might alter the structure of ACE2 and lead to changes in Raman spectra. Additionally, the binding specificity allows ACE2 as an anchor to capture SARS-CoV-2 from human or environmental samples for interrogation.

In this study, we proposed a 'capture-quenching' strategy to rapidly detect SARS-CoV-2 and developed a SERS assay introducing ACE2 functionalized on silver-nanorod SERS substrates to capture and interrogate SARS-CoV-2 spike protein (Fig. 1). We firstly functionalized ACE2 on an aligned silver-nanorod SERS (SN-SERS) array in oblique angle deposition to capture and interrogate SARS-CoV-2 spike protein. The induced SERS signal quenching was documented by either red-shift or whole spectral alterations in multivariate analysis as indicators for the presence of SARS-CoV-2 in real environmental water samples.

2. Materials and methods

2.1. Preparation of silver-nanorod SERS array

The aligned silver-nanorod SERS (SN-SERS) array was fabricated in oblique angle deposition (OAD) using a custom-designed electron beam/sputtering evaporation system (Suzhou Derivative Biotechnology Co., LTD.) and formed randomly on a 4-inch silicon wafer with increasing deposition time (Shanmukh et al., 2006). Briefly, Si-wafer was immersed in absolute alcohol and blow-dried up using N_2 gas prior to loading on the substrate holder. The substrate holder was then fixed on the specially designed Glancing Angle Deposition (GLAD) sample stage in an e-beam evaporator. Deposition was performed at a base pressure lower than 3×10^{-4} Pa. The thickness of film growth was monitored using a quartz crystal microbalance. Firstly, a thin layer of about 20 nm was deposited to assist the adhesion of silver on Si-wafer, followed by the deposition of a base layer of 200 nm silver. The GLAD stage was then tilt to 84° with respect to the incident vapor. A layer of 80 nm was then deposited with substrate rotation at 0.1 rev/s to improve the seeding for nanorod growth. The deposition rate was 2 Å/s in each stage and lasted about 3 h.

2.2. Fabrication of ACE2@SN-SERS substrate

ACE2 was purchased from Novoprotein (China) and stored in borate buffer solution (0.1 M, pH=7.2) at −80 °C before use and the ACE2@SN-SERS substrate was fabricated by Suzhou Yiqing Environmental Science and Technology LTD (China). Briefly, SN-SERS substrate was firstly cleaned by thorough rinse with deionized water and dried using N_2 gas flow. Subsequently, 1 μL of ACE2 stock solution (30 pg) was loaded to SN-SERS substrate and placed in an incubator under constant temperature and humidity conditions (25 °C; 75%, w/w) for 4 h. ACE2 was then bound onto the surface of SN-SERS substrate, designated as ACE2@SN-SERS substrate, which could be stored in 4 °C for 2 weeks before use.

2.3. Water samples and biological analysis

Twenty-three water samples were collected from rivers, hospitals and pipe networks in Wuhan (China) from 24th March to 10th April 2020 (Table 1). Around 2.0 L of water was directly collected in a plexiglass sampler, placed in 4 °C ice-boxes and immediately transferred into laboratory for RNA extraction following our reported protocol (Zhang et al., 2020a). Briefly, after centrifugation at 3000 rpm to remove suspended solids, the supernatant was subsequently supplemented with NaCl (0.3 mol/L) and PEG-6000 (10%), settled overnight at 4 °C, and centrifuged at 10,000 g for 30 min. Viral RNA in pellets was extracted using the EZ1 virus Mini kit (Qiagen, Germany) according to the manufacturer's instructions. SARS-CoV-2 RNA was quantified by RT-qPCR using AgPath-ID™ One-Step RT-PCR Kit (Life Technologies, USA) on a LightCycler 480 Real-time PCR platform (Roche, USA) in duplicates. Two target genes simultaneously amplified were open reading frame lab (CCDC–ORF1, forwards primer: 5′-CCCTGTGGGTTTTACACTTAA-3′; reverse primer: 5′-ACGATTGTGCATCAGCTGA-3′; fluorescence probe: 5′-FAM-CCGTCTGCGGTATGTGGAAAGGTTATGG-BHQ1–3′) and nucleocapsid protein (CCDC–N, forwards primer: 5′-GGGGAACTTCTCCTGCTAGAAT-3′; reverse primer: 5′-CAGACATTTTGCTCTCAAGCTG-3′; fluorescence probe: 5′-FAM-TTGCTGCTGCTTGACAGATT-TAMRA-3′). RT-qPCR amplification for CCDC–ORF1 and CCDC–N was performed in 25 μL reaction mixtures containing 12.5 μL of 2×RT-PCR Buffer, 1 μL of 25×RT-PCR Enzyme Mix, 4 μL mixtures of forward primer (400 nM), reverse primer (400 nM) and probe (120 nM), and 5 μL of template RNA. Reverse transcription was conducted at 45 °C for 10 min (1 cycle), followed by initial denaturation at 90 °C for 10 min (1 cycle) and 40 thermal cycles of 60 °C for 45 second and 90 °C for 15 s. Quantitative fluorescent signal for each sample was normalized by ROX™ passive reference dye provided in 2×RT-PCR buffer. For each RT-qPCR run, both positive and negative controls were included. The copy numbers of SARS-CoV-2 was obtained from a standard calibration curve by a 10-fold serial dilution of genes encoding nucleocapsid protein with an amplification efficiency of 102.6%, calculated as copies=$10^{[-(Cq-39.086)/3.262]}$ (R^2=0.991). For quality control, a reagent blank and extraction blank were included for RNA extraction procedure and no contamination was observed.

2.4. Validation treatment and tests

To validate the performance and specificity of ACE2@SN-SERS substrate, negative controls were prepared and included cells of

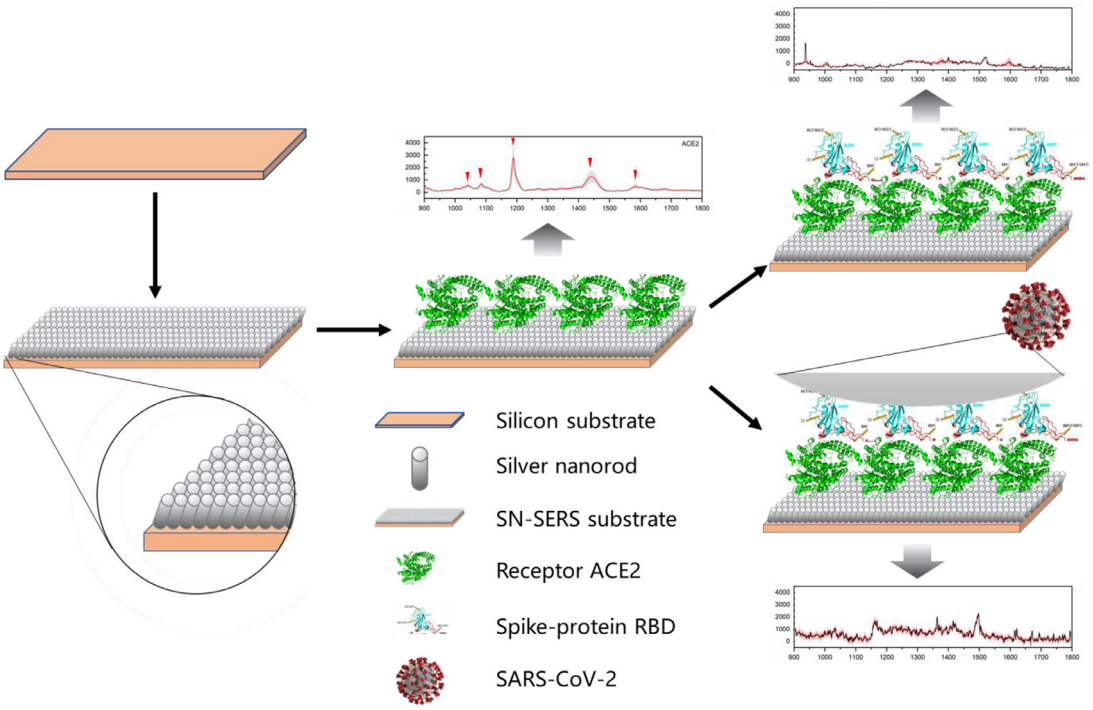

Fig. 1. State-of-the-art diagram of surface enhanced Raman scattering (SERS) for interrogating Severe Acute Respiratory Syndrome Coronavirus 2 (SARS-CoV-2). Human cellular receptor Angiotensin-Converting Enzyme 2 (ACE2) is functionalized on silver-nanorod SERS (SN-SERS) substrate, designated as ACE2@SN-SERS array, which generates strong SERS signals (1032, 1051, 1089, 1189, 1447 and 1527 cm^{-1}). The recognition and binding of receptor binding domain (RBD) of SARS-CoV-2 spike protein on ACE2@SN-SERS assay significantly quenches the spectral intensities of most peaks and exhibits a red-shift from 1189 to 1182 cm^{-1}.

Table 1
Sampling sites and copy numbers of SARS-CoV-2 RNA in water samples.

Location	Samples	Description	SARS-CoV-2
Huoshenshan	HSSCC	Crude water from wards	633 copies/L
Hospital	HSSBC	Water in wastewater treatment plant	Negative
	HSSCD	HSSCC after disinfection	Negative
	HSSBD	HSSBC after disinfection	Negative
Jinyintan	JYTCC	Crude water from wards	255 copies/L
Hospital	JYTCC2	JYTCC after 1-day storage at 20 °C	750 copies/L
	JYTCC3	JYTCC after 3-day storage at 20 °C	3.01×10^3 copies/L
	JYTCD	JYTCC after disinfection	Negative
	JYTBC	Water in wastewater treatment plant	Negative
	JYTBC2	JYTBC after 1-day storage at 20 °C	Negative
	JYTBC3	JYTBC after 3-day storage at 20 °C	Negative
Huanan	HN01	Upstream waters in pipeline	Negative
Seafood	HN02	Upstream waters in pipeline	Negative
Market	HN03	Downstream waters in pipeline	Negative
	HN04	Downstream waters in pipeline	Negative
	HN05	Waters in pipeline joint point	Negative
	HN06	Waters in pipeline joint point	2.88×10^4 copies/L
Rivers	YZRU	20 km upstream waters in Yangtze River	Negative
	YZRM	Waters of Yangtze River in Wuhan city region	Negative
	YZRD	20 km downstream waters in Yangtze River	Negative
	HJRU	10 km upstream waters in Hanjiang River	Negative
	HJRM	Waters of Hanjiang River in Wuhan city region	Negative
	HJRD	Downstream waters at the joint of Hanjiang and Yangtze River	Negative

Escherichia coli DH5α, proteins of *E. coli* DH5α and bacteriophage Phi6. Cells of *E. coli* DH5α were grown in LB medium at 37 °C for 16 hr, harvested by centrifugation, washed three times with deionized water, and finally stored at 4 °C prior to test. Proteins of *E. coli* DH5α cells were extracted after 16-hr cultivation using All-Prep Bacterial Protein Kit (QIAGEN, USA) following manufacturer's instruction, and stored at −20 °C prior to test. Bacteriophage Phi 6 is an enveloped RNA virus widely used for study on viral survival and persistence in environmental media (Whitworth et al., 2020; Wood et al., 2020). It was purchased from DSMZ-German Collection of Microorganisms and Cell Cultures GmbH as vacuum-dried suspensions on filter paper in double-vial glass ampoules. Bacteriophage Phil6 was carefully revitalized by a previous protocol (Whitworth et al., 2020), harvested and purified in the suspension of sterile water, and stored at 4 °C prior to test. SARS-CoV-2 spike proteins were extracted and provided by School of Life Sciences (Tsinghua University) following a reported protocol (Lan et al., 2020).

Five microliters of stock solutions (*E. coli* DH5α cells and bacteriophage Phi6, around 10^3 copies; *E. coli* DH5α proteins and SARS-CoV-2 spike proteins, around 10 pg) and water samples were directly loaded onto the fabricated ACE2@SN-SERS substrate and

incubated at room temperature for 5 min. After dryness, the substrate was ready for Raman spectral acquisition and can be stored at 4 °C for at least 1 week. A series dilution of SARS-CoV-2 spike proteins were used to obtain the qualitative curves between Raman shifts and SARS-CoV-2 spike proteins, ranging from 0.1 pg to 10 pg.

2.5. Raman spectral acquisition

For laboratory test, Raman spectra were acquired using a near-infrared confocal Raman microscope (HR evolution, Horiba, USA) equipped with a 785 nm near-IR laser source, a 300 l/mm grating and a semiconductor-cooling detector (CCD). All Raman spectra were collected with a 50× objective lens (NA=0.7) at an exposure time of 10 s, 3 accumulations, and laser power of 10 mW prior to lens. Raman spectroscopic system was calibrated with a silicon wafer at Raman shift of 520 cm^{-1}. At least five random regions were measured for each sample, and a minimum of 9 individual spectra were acquired per sample. A 785-nm portable Raman spectrometer (Finder Edge, Zolix, China) was used for on-site detection, and the ACE2@SN-SERS substrate was placed on the probe of the portable Raman spectrometer with the following parameters: 0.5 s acquisition time and 300 mW laser power. This portable Raman spectrometer has a satisfactory spectral resolution of 4 cm^{-1} to distinguish possible spectral shift of biological samples. At least five-time measurement was conducted for each sample. For both laboratory and on-site test, all Raman spectra were recorded in the range of 100–3500 cm^{-1} in biological triplicates. On-site spectra acquisition took only 2 min, followed by multivariate analysis for about 3 min to allow overall test within 5 min.

2.6. Multivariate analysis of Raman spectra

Raw spectral data were pre-processed by using the open source IRootLab toolbox performed on MATLAB r2012 (Trevisan et al., 2013). Briefly, each acquired Raman spectrum was cut to a biochemical-cell fingerprint region (900–1800 cm^{-1}), baseline corrected, wavelet de-noised, and vector normalized. Unlike RT-qPCR and immunochromatography assay, our ACE2@SN-SERS assay generates Raman spectral data, which are multivariate and difficult to generate an individual variable for SARS-CoV-2. Thus, we used two approaches to distinguish the difference between positive and negative samples. Firstly, the ratio of Raman intensity at 1182 cm^{-1} to that at 1189 cm^{-1} was calculated, designated as 1182/1189 ratio, as an indicator for positivity prediction. Alternatively, multivariate analysis was applied to the pre-processed spectral data to reduce data dimensions and extract key information. Principal component analysis (PCA) is an unsupervised data analytical method reducing the dimensionality of data, determining principal components (PCs) and extracting key features (Jin et al., 2017; Li et al., 2020a). The first 10 PCs, which account for more than 90% of the variance of the selected spectral regions, were then inputted into linear discriminate analysis (LDA), which determines the discriminant function line that maximizes the inter-class distance and minimizes the intra-class distance to derive an optimal linear boundary separating the different classes. Generally, PCA-LDA score plots and cluster vectors are generated, and the scores of the linear discriminant 1 (LD1) provides the best classification (Li et al., 2020a).

2.7. Statistical analysis

One-way ANOVA was used to compare the difference between samples and p-value less than 0.05 refers to statistically significant difference.

3. Results and discussions

3.1. Features of SN-SERS and ACE2@SN-SERS substrates

SEM images (Fig. 2A) illustrated a successful fabrication of silver nanorods on SERS substrate. The overall diameter and length of silver nanorods was 211±45 and 737±52 nm, respectively, and the uniform structure demonstrated a density of 8 nanorods/μm^2. After functionalization with ACE2 protein, clear protein structures were observed on ACE2@SN-SERS substrate, exhibiting as small islands with a diameter of 2 μm (Fig. 2B).

The background Raman signals of SN-SERS substrate without ACE2 exhibited no significant peaks from 900 to 1800 cm^{-1} (Figure S1), showing a satisfactory performance for interrogating bio-related SERS. ACE2@SN-SERS substrate generated remarkable SERS signals, around 400 times stronger than SN-SERS substrate (Figure S1). The featured Raman peaks are probably assigned with phenylalanine (1032 cm^{-1}) (Rygula et al., 2013), C–N stretching in protein (1089 cm^{-1}) (Chan et al., 2006), Amide III for C–N stretching and N–H bending (1189 cm^{-1}) (Malini et al., 2006), CH_2 bending mode of proteins (1447 cm^{-1}) (Ó Faoláin et al., 2005) and conjugated -C = C- in protein (1587 cm^{-1}) (Rau et al., 2016).

3.2. SERS detection of SARS-CoV-2 spike protein

SARS-CoV-2 spike protein was firstly tested on SN-SERS and ACE2@SN-SERS substrates as a proof-of-concept demonstration. Different from ACE2 protein, Raman peak intensities derived from SARS-CoV-2 spike protein were relatively weak on SN-SERS substrate and the distinct peaks were mostly located at 1032, 1051, 1182, 1447 and 1597 cm^{-1} (Fig. 2C). They are probably assigned to phenylalanine (1032 cm^{-1}) (Rygula et al., 2013), C–N stretching in protein (1051 cm^{-1}) (Chan et al., 2006),––CH_2 bending mode of proteins (1447 cm^{-1}) (Ó Faoláin et al., 2005). After loading spike proteins onto ACE2@SN-SERS substrate, the whole spectra exhibited a quenching of SERS signal intensity, especially at Raman shifts of 1089, 1189 and 1447 cm^{-1} (Fig. 2C).

SARS-CoV-2 spike protein RBD targets the short β5 and β6 strands, α4 and α5 helices and loops on ACE2 (Lan et al., 2020), which are rich in phenylalanine and Amide III for C–N stretching and N–H bending, and the networks of hydrophilic interactions at RBD/ACE2 interfaces quench their SERS signals at 1032 cm^{-1} and 1189 cm^{-1}. Particularly, a red-shift from 1189 to 1182 cm^{-1} representing N–H bending was observed, possibly attributing to the direct enhancement of 1182 cm^{-1} from SARS-CoV-2 spike protein. Raman intensities of peak 1189 cm^{-1} of ACE2@SN-SERS substrate (2552±163 arbitrary unit) were about 2 times as those of peak 1182 cm^{-1} (1354±76 arbitrary unit), whereas the peak intensities of 1182 cm^{-1} (430±10 arbitrary unit) were higher than those of 1189 cm^{-1} (290±11 arbitrary unit) postexposure to SARS-CoV-2 spike proteins. It is possibly induced by the change in N–H vibration mode or the bond length of N–H (Rozenberg et al., 2000; Tomobe et al., 2017), in response to the interfered H-bond of ACE2 after recognizing SARS-CoV-2 spike protein. In addition, the intensities of both peaks 1189 cm^{-1} and 1182 cm^{-1} were positively correlated with the dosage of SARS-CoV-2 proteins (Figure S2A), and the 1182/1189 ratios of SERS signals exhibited a positive correlation with the dosage of SARS-CoV-2 spike proteins (Figure S2B). In contrast, there was no Raman shift from 1189 to 1182 cm^{-1} in all the treatments with bacteriophage Phi6, whole cells of *E. coli*, and extracted proteins of *E. coli* cells (Fig. 2D). Besides 1189 cm^{-1}, all these treatments produced identical peaks of 1094, 1161, 1249, 1311 and 1412 cm^{-1}, representing typical biospectral alterations of amino acids, phosphorylated proteins, cellular nucleic acids, fatty acids and lipids (Jin et al., 2020; Li et al., 2017). These results indi-

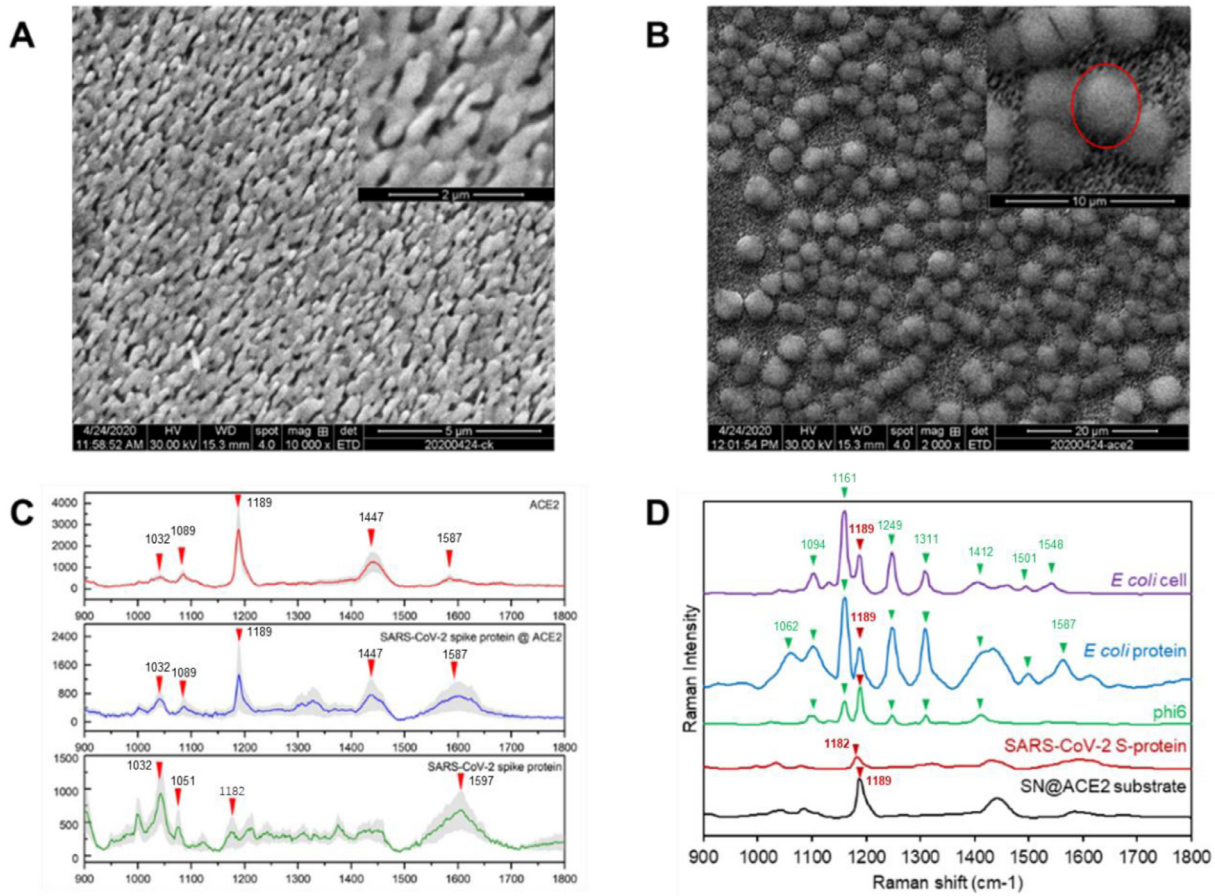

Fig. 2. (A) SEM image of SN-SERS substrate. Scale bar: 5 μm (upper right: 2 μm). (B) SEM image of ACE2@SN-SERS substrate. Scale bar: 20 μm (upper right: 10 μm). Functionalized ACE2 protein is present as 'islands' (red circle). (C) Comparison of SERS signals between ACE2@SN-SERS substrate, SARS-Co-2 spike protein with ACE2, and SARS-CoV-2 spike protein on SN-SERS substrate. Featured SERS signals of ACE2 protein include 1032, 1089, 1189, 1447 and 1587 cm^{-1}. (D) Comparison of SERS signals between SARS-CoV-2 spike protein, bacteriophage Phi6, whole cells of *E. coli*, and extracted proteins of *E. coli* cells on ACE2@SN-SERS substrate. Only SARS-CoV-2 spike protein represents Raman shift from 1189 to 1182 cm^{-1}.

cated that the fabricated ACE2@SN-SERS substrate can specifically recognize SARS-CoV-2 spike protein and there is neglectable interference from other enveloped viruses or bacterial cells. Our results indicated that SARS-CoV-2 spike protein can be recognized and bound by ACE2@SN-SERS substrate, consequently changing ACE2 structure to induce the SERS signal quenching. Such significant Raman signal change demonstrated that our designed ACE2@SN-SERS assay has a satisfactory performance in SARS-CoV-2 interrogation. Either 1189 cm^{-1} intensity, 1182 cm^{-1} intensity or 1182/1189 ratio could quantitatively interrogate the presence of SARS-CoV-2 spike proteins.

3.3. Interrogation of SARS-CoV-2 in real water samples from Wuhan via ACE2@SN-SERS

In on-site test, Raman spectra of ACE2 acquired via the portable Raman spectrometer exhibited coherent spectral peaks presented at 1032, 1089, 1189, 1447 and 1587 cm^{-1} comparing to those from the research-level Raman spectrometer in laboratory, although relatively high signal noises were observed. It indicated the robustness of our developed ACE2@SN-SERS array and feasibility for on-site detection. Raman spectra of water samples on ACE2@SN-SERS array exhibited different SERS signals (Fig. 3A). Detailed spectral region from 1170 to 1200 cm^{-1} illustrated that some samples had significant signal quenching at 1189 cm^{-1} (Figure S3), e.g., JYTCC, JYTCC2, JYTCC3, HSSCC, HSSBC and HN06, whereas others possessing similar spectral patterns as ACE2@SN-SERS array included HSSCD, HSSBD, etc.

RT-qPCR results had separated all water samples into positive and negative groups for SARS-CoV-2. To distinguish these two groups from SERS spectra, we first used 1182/1189 ratio as an indicator, as the red-shift from 1189 to 1182 cm^{-1} was the most remarkable spectral alteration. Fig. 3C shows a significant difference in 1182/1189 ratio between positive and negative groups ($p<0.001$), averagely 1.311±0.446 and 0.766±0.218, respectively. When 1182/1189 ratio ranges from 0.800 to 1.100, the false-positive percentage slightly decreases from 20.0% to 0.0%, whereas the false-negative percentage increases from 0.0% to 40.0%. Accordingly, the highest accuracy of 1182/1189 ratio is 93.33% when the threshold is 1.000, and the false-positive and false-negative percentage is 10.0% and 0.0%, respectively (Figure S4A). Thus, 1182/1189 ratio is a satisfactory indictor to detect the presence of SARS-CoV-2 in water samples.

Nevertheless, the intrinsic SERS analysis provided convoluted Raman signals derived from ACE2 proteins or complexes of ACE2 and spike protein of SARS-CoV-2 located in plasmonic hot spot regions, and it is crucial to employ multivariate method to extract information in these complex multivariable spectroscopic data for a better interrogation. Herein, the whole spectra from 900 to 1800 cm^{-1} were analyzed by PCA-LDA, and the score plot clearly segregates the positive and negative groups (Fig. 3B). LD1 derived from PCA-LDA model provided the best classification, mainly representing the shift of 1189 to 1182 cm^{-1} and the declining peaks at 1089

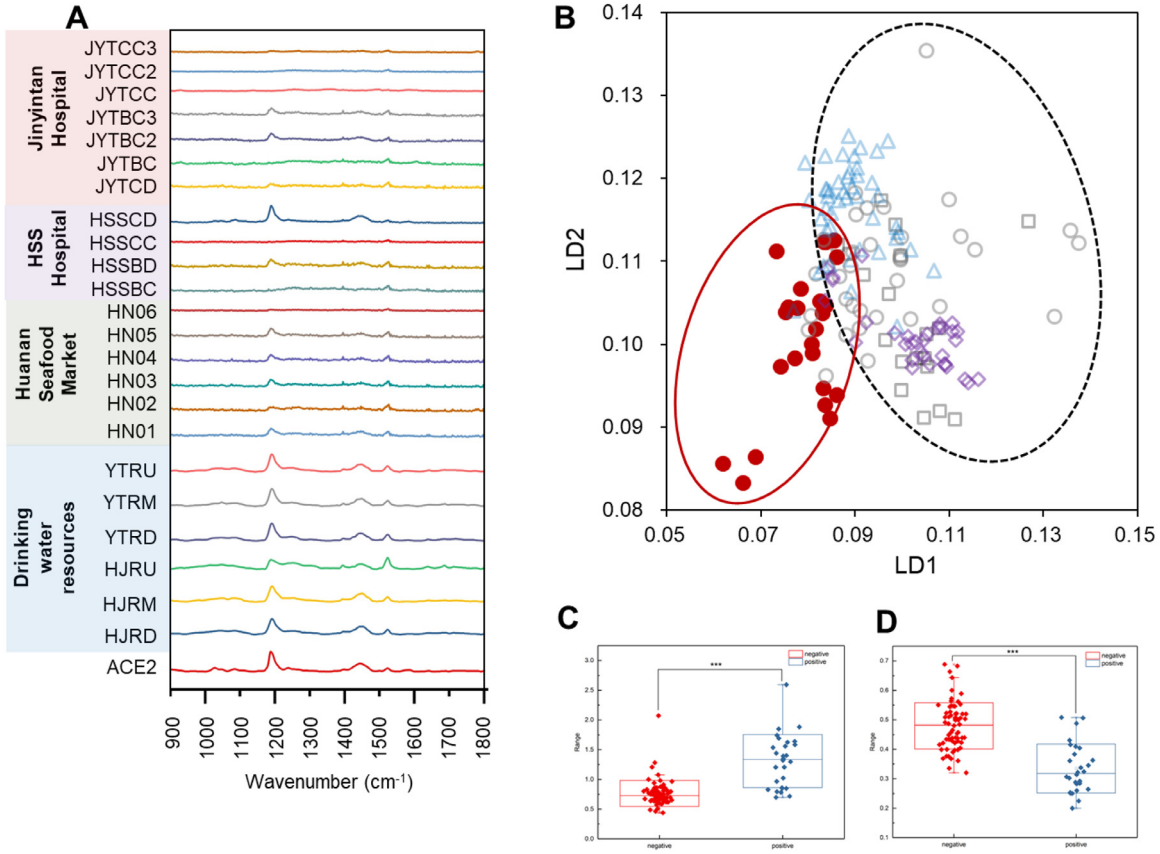

Fig. 3. (A) SERS spectra of ACE2@SN-SERS and 23 tested water samples by ACE2@SN-SERS assay (mean value) using a portable Raman spectrometer. (B) Segregation of positive and negative water sample groups in PCA-LDA score plot. Red dots represent positive water samples for SARS-CoV-2. □, ○, Δ and ◊ refer to negative water samples collected from wastewater disinfected units, hospitals, rivers and Huanan Seafood Market, respectively. (C) Difference of 1182/1189 ratio between positive and negative groups. (D) Difference of LD1 scores between positive and negative groups.

and 1447 cm^{-1}. In addition, LD2 also explained a small proportion of variance between positive and negative samples, consisting of peaks at 1032 and 1587 cm^{-1}. Accordingly, LD1 scores are assigned as criteria and exhibit significant difference between the positive and negative groups (Fig. 3D, $p<0.001$). When LD1 scores range from 0.070 to 0.120, the false-positive percentage slightly increases from 0.0% to 20.0%, whereas the false-negative percentage decreases from 40.0% to 0.0%. Accordingly, the highest accuracy of LD1 scores is 93.33% when the threshold is 0.080 (Figure S4B).

Further analysis on the spectral region from 1170 to 1200 cm^{-1} (Figure S3) explained the potential reason for false-positive and false-negative measurement, that some sample exhibited both shift from 1189 to 1182 cm^{-1} and considerable intensities at 1189 cm^{-1}. It might be explained by the limited number of SARS-CoV-2 protein in environmental samples that could not completely quench SERS signals of ACE2 (false-negative) or binding of similar proteins with ACE2 to raise the intensities at 1182 cm^{-1} (false positive). From the results of duplicated measurements for each sample, the consistency and repeatability of this SERS assay is 0.853 (Kendall coordination coefficient, $p<0.01$) and 4.5% (relative standard deviation, RSD) based on 1182/1189 ratio and 0.892 (Kendall coordination coefficient, $p<0.01$) and 4.2% (RSD) based on LD1 scores, respectively. Although the concept of using Raman spectroscopy to detect SARS-CoV-2 viruses has been raised by many researchers (Lukose et al., 2021), these studies mainly focus on the detection sensitivity or substrate fabrication with artificial samples and there is no report on the detection of real environmental samples or accuracy (Jadhav et al., 2021; Peng et al., 2021). Our findings proved the feasibility of ACE2@SN-SERS assay to on-site interrogate SARS-CoV-2 in real water samples, and both indicators have satisfactory performance.

3.4. Tracking and explaining the presence of SARS-CoV-2 in environmental water samples via on-site interrogation

SARS-CoV-2 in crude water from wards of Huoshenshan Hospital (HSSCC) and Jinyintan Hospital (JYTCC) was 633 copies/L and 255 copies/L, respectively, showing the presence of SARS-CoV-2 viral RNA. The results became negative in the biological treatment sector (HSSBC) and aerobic biodegradation sector (JYTBC) in the wastewater treatment plants of Huoshenshan and Jinyintan Hospitals (Table 1). However, both 1182/1189 ratios and LD1 scores by ACE2@SN-SERS assay had contradictory results that SARS-CoV-2 was present in all wastewater samples throughout in the treatment process despite of slight decay (Fig. 4A and 4E). It might be explained by higher stability of SARS-CoV-2 spike protein than RNA after disinfection, and the residual spike proteins were still detectable but the infectivity was of low risk. Our findings indicated a decay of SARS-CoV-2 viral RNA along wastewater treatment process, consistent with previous reported facts that both RNA (Norovirus GGI, GGII, sapovirus, and Aichi virus) and DNA viruses (enteric adenoviruses, JC polyomaviruses, BK polyomaviruses) were effectively removed in conventional and biological wastewater treatment plants (Hata et al., 2013; Kitajima et al., 2014; Nordgren et al., 2009). The presence of SARS-CoV-2 in the adjusting tanks might pose threats to workers for medical wastewater treatment, and their personal care protections are suggested

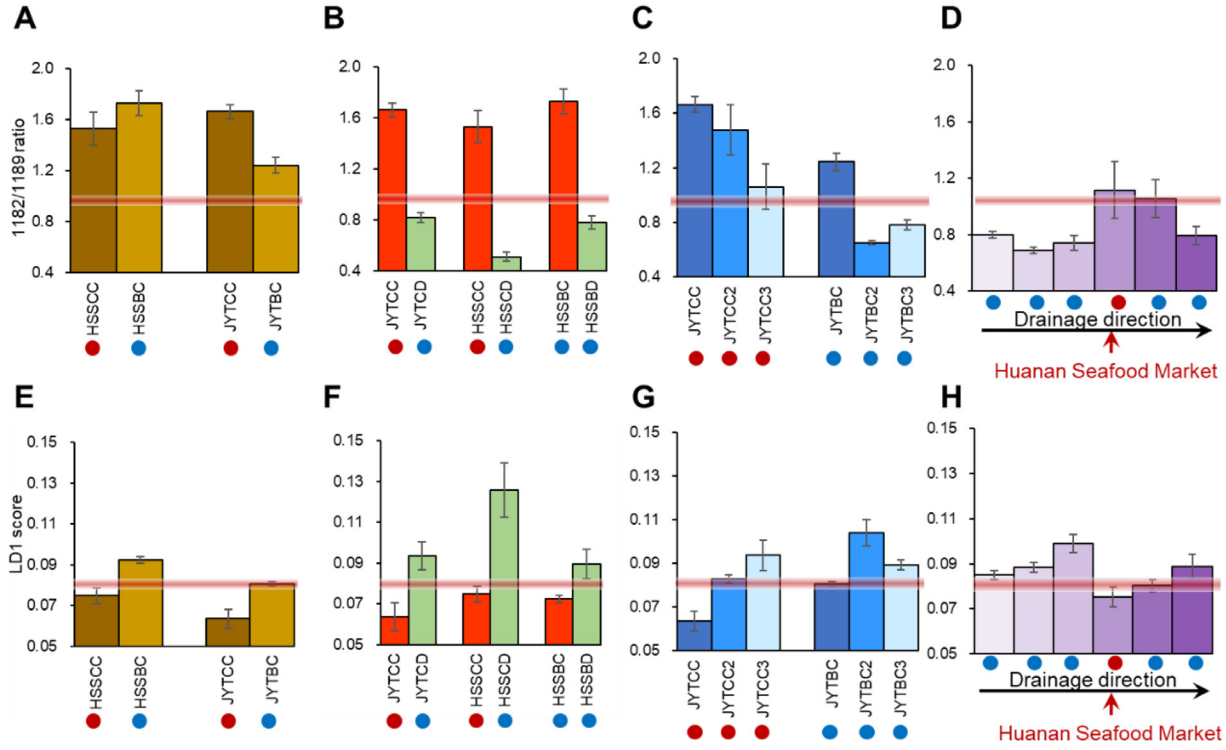

Fig. 4. Applications of on-site SERS interrogation for SARS-CoV-2. Change of 1182/1189 ratio (A) and LD1 score (E) along wastewater treatment process for wastewater treatment plant management. Significant difference of 1182/1189 ratio (B) and LD1 score (F) between crude and disinfected waters for determination of disinfection efficiency. Change of 1182/1189 ratio (C) and LD1 score (G) for viral survival in environmental media. Occurrence of SARS-CoV-2 in the pipeline of Huanan Seafood Market by 1182/1189 ratio (D) and LD1 score (H). Red and blue dots indicated water samples with positive and negative qPCR results for SARS-CoV-2.

to prevent potential infection. The rapidness and easy operation of this developed ACE2@SN-SERS assay offers a solution to monitor SARS-CoV-2 in medical wastewater treatment plants, allowing on-site assessment of potential spreading risks on workers and surrounding environment.

Disinfection completely removed SARS-CoV-2 viral RNA, exhibiting negative RT-qPCR and ACE2@SN-SERS results for disinfected water (HSSCD, HSSBD and JYTCD, Fig. 4B and 4F). LD1 scores by ACE2@SN-SERS assays also suggested the existence of SARS-CoV-2 after 1 to 3 days storage (Fig. 4C and 4G), consistent with the results of RT-qPCR (750 and 3.01×10^3 copies/L). These results proved the robustness of ACE2@SN-SERS assay in detecting SARS-CoV-2 in real water samples, offering strong evidence to document the effective disinfection performance (Kampf et al., 2020) and long-term survival for at least 3 days (van Doremalen et al., 2020).

Diagnosing confirmed patients and tracking asymptomatic candidates is one of major challenges for COVID-19 prevention and control. In this work, we collected water samples from pipeline receiving discharge from Huanan Seafood Market, a suspected first place of COVID-19 outbreak in China. The upstream waters had negative RT-qPCR results and exhibited no SARS-CoV-2 spike protein from clear Raman shifts at 1189 cm^{-1} in ACE2@SN-SERS assay (Fig. 3A). After receiving wastewater from Huanan Seafood Market, the positive RT-qPCR results (2.88×10^4 copies/L, Table 1), 1182/1189 ratios (Fig. 4D) and LD1 scores (Fig. 4H) illustrated the entry of SARS-CoV-2 into pipelines. Different from RT-qPCR assay requiring RNA extraction and laboratory amplification, the developed ACE2@SN-SERS assay allows onsite detection of SARS-CoV-2 with portable Raman spectrometers, showing huge potentials for field practices to track the presence and source of SARS-CoV-2 in sewage pipe network.

All water samples collected from Yangtze and Hanjiang River did not exhibited significant Raman shift from1189 cm^{-1} to 1182 cm^{-1} (Fig. 3A), consistent with qPCR results (Table 1). These results indicated that no SARS-CoV-2 was detectable in surface waters and its spreading risk through natural rivers are neglectable. Although both Yangtze River and Hanjiang River received treated discharge from wastewater treatment plants in Wuhan, which had influents containing SARS-CoV-2 (Fig. 4A), disinfection can effectively remove viral RNA (Fig. 4B) and leave limited risks of SARS-CoV-2 spillover into natural environment. The occurrence of SARS-CoV-2 in wastewater and rivers has been reported in Paris (Rimoldi et al., 2020), and its potential transmission and spread in the urban and rural water cycle might pose threats to public health (Bhowmick et al., 2020). For rivers or lakes receiving untreated sewage, this ACE2@SN-SERS assay might be a solution for rapidlya and online detecting SARS-CoV-2 viral RNA for drinking water safety.

3.5. Prospective

The developed ACE2@SN-SERS assay provides good accuracy and satisfactory performance for the rapid and onsite detection of SARS-CoV-2 in environmental specimens, meeting well with RT-qPCR results. Compared with RT-qPCR and immunochromatography assays, this ACE2@SN-SERS assay has three advantages. Firstly, ACE2@SN-SERS assay does not rely on RNA extraction or immune biomarker, simplifying the sample preparation procedure and shortening the measurement time. Secondly, spike protein is more stable than RNA as the biomarker for SARS-CoV-2, hinting a more stable and sensitive assay particularly for environmental specimens. Last but not the least, we have proved that portable Raman spectrometers can provide satisfactory signals with ACE2@SN-SERS assay and allows rapid interrogation of SARS-CoV-2 on site.

There are some limitations in this work. Firstly, our ACE2@SN-SERS assay cannot evaluate viral viability or infectivity as free spike proteins or viral envelop are also recognizable by ACE2@SN-

SERS substrates to quench SERS signals, possibly overestimating the presence of SARS-CoV-2 in human or environmental specimens. Secondly, only limited real samples were tested and the interference of other viruses targeting ACE2 for cell entry is still questionable, owing to the restriction in sample collection and clinical tests during the outbreak of COVID-19 in Wuhan. On the contrary, the mentioned advantages prove ACE2@SN-SERS assay as a reliable and mobile detection platform or screening system for onsite clinal and environmental detection under a variety of conditions. Thirdly, we did not get resources to measure the effects of other viruses (e.g., SARS-CoV-1) or antigens of influenza virus A/B and SARS-CoV-2 targeting ACE2 proteins. From the interrogation mechanisms, they might activate SERS response and produce false-positive signals for SARS-CoV-2 detection, which reduces the specificity of this SERS assay. Instead, our state-of-the-art work also raises a concept to screen other viruses with RBD recognizing receptors of human cells for entry and evaluate the recognition strength of SARS-like viruses across mammalian species, when different RBD-containing viruses are tested or human cell receptors are functionalized for substrate fabrication. As a possible in-vitro assay, ACE2@SN-SERS substrate might also contribute to the assessment of vaccine efficiency. Further studies need to address those possibilities and establish robust databases and algorithms for a faster interrogation, even down to 1 min, for clinical and environmental purposes.

4. Conclusion

A novel ACE2@SN-SERS assay was developed in this study by functionalizing human cellular receptor ACE2 proteins on silver-nanorods and generating strong SERS signals. The successful and significant quenching of SERS signal intensities in the presence of SARS-CoV-2 spike proteins proved its capability in capturing and recognizing SARS-CoV-2. Onsite tests on 23 water samples using a portable Raman spectrometer achieved satisfactory performance in interrogating the presence of SARS-CoV-2 in environmental specimens, although some inconsistent with RT-qPCR results. At the current stage, the developed ACE2@SN-SERS assay had acceptable accuracy, false-positive and false-negative percentages, which can be further improved by fabrication implementation, database set-up and algorithm optimization. It has a bright future and huge potential as a rapid and on-site detection tool for SARS-CoV-2 and other viruses to confirm patients, determine community cases and track environmental viral sources in pandemics.

Declaration of Competing Interest

The authors declare that they have no known competing financial interests or personal relationships that could have appeared to influence the work reported in this paper.

Acknowledgement

The authors would like to thank the projects from the Major Program of National Natural Science Foundation of China (52091543) and Chinese Academy of Engineering (2020-ZD-15) for providing water samples, and Science and Technology Service Network Initiatives (KFJ-STS-QYZX-061) and Scientific Research Equipment Development Project (YZ201653) for SN-SERS substrate fabrication. DZ also acknowledges the support of Chinese Government's Thousand Talents Plan for Young Professionals.

Supplementary materials

Supplementary material associated with this article can be found, in the online version, at doi:10.1016/j.watres.2021.117243.

References

Amanat, F., Stadlbauer, D., Strohmeier, S., Nguyen, T., Chromikova, V., McMahon, M., Jiang, K., Asthagiri-Arunkumar, G., Jurczyszak, D., Polanco, J., Bermudez-Gonzalez, M., Kleiner, G., Aydillo, T., Miorin, L., Fierer, D., Lugo, L.A., Kojic, Milunka, E., Stoever, J., Liu, S.T.H., Cunningham-Rundles, C., Felgner, P.L., Caplivski, D., Garcia-Sastre, A., Cheng, A., Kedzierska, K., Vapalahti, O., Hepojoki, J., Simon, V., Krammer, F., Moran, 2020. A Serological Assay to Detect SARS-CoV-2 Seroconversion in Humans, 26. Nature Medicine, pp. 1033–1036.

Auta, H.S., Emenike, C.U., Fauziah, S.H., 2017. Distribution and importance of microplastics in the marine environment: a review of the sources, fate, effects, and potential solutions. Environ. Int. 102, 165–176.

Bhowmick, G.D., Dhar, D., Nath, D., Ghangrekar, M.M., Banerjee, R., Das, S., Chatterjee, J., 2020. Coronavirus disease 2019 (COVID-19) outbreak: some serious consequences with urban and rural water cycle. npj Clean Water 3 (1), 1–8.

Carlos, W.G., Dela Cruz, C.S., Cao, B., Pasnick, S., Jamil, S., 2020. Novel Wuhan (2019-nCoV) coronavirus. Am. J. Respir. Crit. Care Med. 201 (4) P7-P8.

Chan, J.F.W., Yuan, S.F., Kok, K.H., To, K.K.W., Chu, H., Yang, J., Xing, F.F., Liu, J.L., Yip, C.C.Y., Poon, R.W.S., Tsoi, H.W., Lo, S.K.F., Chan, K.H., Poon, V.K.M., Chan, W.M., Ip, J.D., Cai, J.P., Cheng, V.C.C., Chen, H.L., Hui, C.K.M., Yuen, K.Y., 2020. A familial cluster of pneumonia associated with the 2019 novel coronavirus indicating person-to-person transmission: a study of a family cluster. Lancet 395 (10223), 514–523.

Chan, J.W., Taylor, D.S., Zwerdling, T., Lane, S.M., Ihara, K., Huser, T., 2006. Micro-Raman spectroscopy detects individual neoplastic and normal hematopoietic cells. Biophys. J. 90 (2), 648–656.

Chang, D., Lin, M., Wei, L., Xie, L., Zhu, G., Cruz, Dela, C.S., Sharma, 2020. Epidemiologic and clinical characteristics of novel coronavirus infections involving 13 patients outside Wuhan, China. JAMA 323 (11), 1092–1093.

Hata, A., Kitajima, M., Katayama, H., 2013. Occurrence and reduction of human viruses, F-specific RNA coliphage genogroups and microbial indicators at a full-scale wastewater treatment plant in Japan. J. Appl. Microbiol. 114 (2), 545–554.

Jadhav, S.A., Biji, P., Panthalingal, M.K., Krishna, C.M., Rajkumar, S., Joshi, D.S., Sundaram, N., 2021. Development of integrated microfluidic platform coupled with surface-enhanced Raman spectroscopy for diagnosis of COVID-19. Med. Hypotheses 146, 110356.

Jin, N., Paraskevaidi, M., Semple, K.T., Martin, F.L., Zhang, D.Y., 2017. Infrared spectroscopy coupled with a dispersion model for quantifying the real-time dynamics of kanamycin resistance in artificial microbiota. Anal. Chem. 89 (18), 9814–9821.

Jin, N.F., Morais, C.L.M., Martin, F.L., Zhang, D.Y., 2020. Spectrochemical identification of kanamycin resistance genes in artificial microbial communities using Clover-assay. J Pharmaceut. Biomed. 181, 113108.

Jung, Y.J., Park, G.-.S., Moon, J.H., Ku, K., Beak, S.-.H., Kim, S., Park, E.C., Park, D., Lee, J.-.H., Byeon, C.W., Lee, J.J., Maeng, J.-.S., Kim, S.J., Kim, S.I., Kim, B.-.T., Lee, M.J., Kim, H.G., 2020. Comparative Analysis of Primer-Probe Sets for the Laboratory Confirmation of SARS-CoV-2. bioRxiv 2020.2002.2025.964775.

Kampf, G., Todt, D., Pfaender, S., Steinmann, E., 2020. Persistence of coronaviruses on inanimate surfaces and their inactivation with biocidal agents. J. Hosp. Infect. 104 (3), 246–251.

Kitajima, M., Iker, B.C., Pepper, I.L., Gerba, C.P., 2014. Relative abundance and treatment reduction of viruses during wastewater treatment processes–identification of potential viral indicators. Sci. Total Environ. 488-489, 290–296.

Lai, C.-.C., Shih, T.-.P., Ko, W.-.C., Tang, H.-.J., Hsueh, P.-.R., 2020. Severe acute respiratory syndrome coronavirus 2 (SARS-CoV-2) and coronavirus disease-2019 (COVID-19): the epidemic and the challenges. Int J Antimicrob Agents 55 (3), 105924.

Lan, J., Ge, J., Yu, J., Shan, S., Zhou, H., Fan, S., Zhang, Q., Shi, X., Wang, Q., Zhang, L., 2020. Structure of the SARS-CoV-2 spike receptor-binding domain bound to the ACE2 receptor. Nature 581 (7807), 215–220.

Li, H.B., Martin, F.L., Zhang, D.Y., 2017. Quantification of chemotaxis-related alkane accumulation in acinetobacter baylyi using Raman microspectroscopy. Anal. Chem. 89 (7), 3909–3918.

Li, H.B., Zhang, D.Y., Luo, J., Jones, K.C., Martin, F.L., 2020a. Applying Raman microspectroscopy to evaluate the effects of nutrient cations on alkane bioavailability to acinetobacter baylyi ADP1. Environ. Sci. Technol. 54 (24), 15800–15810.

Li, Q., Guan, X., Wu, P., Wang, X., Zhou, L., Tong, Y., Ren, R., Leung, K.S.M., Lau, E.H.Y., Wong, J.Y., Xing, X., Xiang, N., Wu, Y., Li, C., Chen, Q., Li, D., Liu, T., Zhao, J., Liu, M., Tu, W., Chen, C., Jin, L., Yang, R., Wang, Q., Zhou, S., Wang, R., Liu, H., Luo, Y., Liu, Y., Shao, G., Li, H., Tao, Z., Yang, Y., Deng, Z., Liu, B., Ma, Z., Zhang, Y., Shi, G., Lam, T.T.Y., Wu, J.T., Gao, G.F., Cowling, B.J., Yang, B., Leung, G.M., Feng, Z., 2020b. Early transmission dynamics in Wuhan, China, of novel coronavirus–infected pneumonia. New Engl. J. Med. 382 (13), 1199–1207.

Lukose, J., Chidangil, S., George, S.D., 2021. Optical technologies for the detection of viruses like COVID-19: progress and prospects. Biosens. Bioelectron. 178, 113004.

Malini, R., Venkatakrishna, K., Kurien, J., Pai, M., K., Rao, L., Kartha, V.B., Krishna, 2006. Discrimination of normal, inflammatory, premalignant, and malignant oral tissue: a Raman spectroscopy study. Biopolymers 81 (3), 179–193.

Morais, C.L.M., Paraskevaidi, M., Cui, L., Fullwood, N.J., Isabelle, M., Lima, K.M.G., Martin-Hirsch, P.L., Sreedhar, H., Trevisan, J., Walsh, M.J., Zhang, D.Y., Zhu, Y.G., Martin, F.L., 2019. Standardization of complex biologically derived spectrochemical datasets. Nat. Protoc. 14 (5), 1546–1577.

Moskovits, M., 1985. Surface-enhanced spectroscopy. Rev. Mod. Phys. 57 (3), 783–826.

Nalla, A.K., Casto, A.M., Huang, M.-L.W., Perchetti, G.A., Sampoleo, R., Shrestha, L., Wei, Y., Zhu, H., Jerome, K.R., Greninger, A.L., 2020. Comparative performance of SARS-CoV-2 detection assays using seven different primer/probe sets and one assay kit. J. Clin. Microbiol. JCM.00557-00520.

Nam, W., Ren, X., Tali, S.A.S., Ghassemi, P., Kim, I., Agah, M., Zhou, W., 2019. Refractive-index-insensitive nanolaminated SERS substrates for label-free raman profiling and classification of living cancer cells. Nano Lett. 19 (10), 7273–7281.

Nolan, T., Hands, R.E., Bustin, S.A., 2006. Quantification of mRNA using real-time RT-PCR. Nat. Protoc. 1 (3), 1559–1582.

Nordgren, J., Matussek, A., Mattsson, A., Svensson, L., Lindgren, P.E., 2009. Prevalence of norovirus and factors influencing virus concentrations during one year in a full-scale wastewater treatment plant. Water. Res. 43 (4), 1117–1125.

Ó Faoláin, E., Hunter, M.B., Byrne, J.M., Kelehan, P., McNamara, M., Byrne, H.J., Lyng, F.M., 2005. A study examining the effects of tissue processing on human tissue sections using vibrational spectroscopy. Vib. Spectrosc. 38 (1), 121–127.

Ong, S.W.X., Tan, Y.K., Chia, P.Y., Lee, T.H., Ng, O.T., Wong, M.S.Y., Marimuthu, K., 2020. Air, surface environmental, and personal protective equipment contamination by severe acute respiratory syndrome coronavirus 2 (SARS-CoV-2) from a symptomatic patient. JAMA 323 (16), 1610–1612.

Peng, Y.S., Lin, C.L., Long, L., Masaki, T., Tang, M., Yang, L.L., Liu, J.J., Huang, Z.R., Li, Z.Y., Luo, X.Y., Lombardi, J.R., Yang, Y., 2021. Charge-transfer resonance and electromagnetic enhancement synergistically enabling MXenes with excellent SERS sensitivity for SARS-CoV-2 S protein detection. Nano-Micro Lett. 13 (1), 52.

Poon, L.L.M., Peiris, M., 2020. Emergence of a novel human coronavirus threatening human health. Nat. Med. 1–2.

Rau, J.V., Graziani, V., Fosca, M., Taffon, C., Rocchia, M., Crucitti, P., Pozzilli, P., Onetti Muda, A., Caricato, M., Crescenzi, A., 2016. RAMAN spectroscopy imaging improves the diagnosis of papillary thyroid carcinoma. Sci. Rep. 6 (1), 35117.

Rimoldi, S.G., Stefani, F., Gigantiello, A., Polesello, S., Comandatore, F., Mileto, D., Maresca, M., Longobardi, C., Mancon, A., Romeri, F., 2020. Presence and infectivity of SARS-CoV-2 virus in wastewaters and rivers. Sci. Total Environ. 744, 140911.

Rozenberg, M., Loewenschuss, A., Marcus, Y., 2000. An empirical correlation between stretching vibration redshift and hydrogen bond length. Phys. Chem. Chem. Phys. 2 (12), 2699–2702.

Rygula, A., Majzner, K., Marzec, K.M., Kaczor, A., Pilarczyk, M., Baranska, M., 2013. Raman spectroscopy of proteins: a review. J. Raman Spectrosc. 44 (8), 1061–1076.

Schmittgen, T.D., Livak, K.J., 2008. Analyzing real-time PCR data by the comparative CT method. Nat. Protoc. 3 (6), 1101–1108.

Shanmukh, S., Jones, L., Driskell, J., Zhao, Y., Dluhy, R., Tripp, R.A., 2006. Rapid and sensitive detection of respiratory virus molecular signatures using a silver nanorod array SERS substrate. Nano Lett. 6 (11), 2630–2636.

Stadlbauer, D., Amanat, F., Chromikova, V., Jiang, K., Strohmeier, S., Arunkumar, G.A., Tan, J., Bhavsar, D., Capuano, C., Kirkpatrick, E., Meade, P., Brito, R.N., Teo, C., McMahon, M., Simon, V., Krammer, F., 2020. SARS-CoV-2 seroconversion in humans: a detailed protocol for a serological assay, antigen production, and test setup. Curr. Protoc. Microbiol. 57 (1), e100.

Stiles, P.L., Dieringer, J.A., Shah, N.C., Van Duyne, R.P., 2008. Surface-enhanced Raman spectroscopy. Rev. Anal. Chem. 1 (1), 601–626.

Tomobe, K., Yamamoto, E., Kojić, D., Sato, Y., Yasui, M., Yasuoka, K., 2017. Origin of the blueshift of water molecules at interfaces of hydrophilic cyclic compounds. Sci. Adv. 3 (12), e1701400.

Trevisan, J., Angelov, P.P., Scott, A.D., Carmichael, P.L., Martin, F.L., 2013. IRootLab: a free and open-source MATLAB toolbox for vibrational biospectroscopy data analysis. Bioinformatics 29 (8), 1095–1097.

van Doremalen, N., Bushmaker, T., Morris, D.H., Holbrook, M.G., Gamble, A., Williamson, B.N., Tamin, A., Harcourt, J.L., Thornburg, N.J., Gerber, S.I., Lloyd-Smith, J.O., de Wit, E., Munster, V.J., 2020. Aerosol and surface stability of SARS-CoV-2 as compared with SARS-CoV-1. New Engl. J. Med. 382 (16), 1564–1567.

Vendrell, M., Maiti, K.K., Dhaliwal, K., Chang, Y.-.T., 2013. Surface-enhanced Raman scattering in cancer detection and imaging. Trends Biotechnol. 31 (4), 249–257.

Wang, D., Hu, B., Hu, C., Zhu, F., Liu, X., Zhang, J., Wang, B., Xiang, H., Cheng, Z., Xiong, Y., Zhao, Y., Li, Y., Wang, X., Peng, Z., 2020. Clinical characteristics of 138 hospitalized patients with 2019 novel coronavirus–infected pneumonia in Wuhan, China. JAMA 323 (11), 1061–1069.

Weiss, S., Klingler, J., Hioe, C., Amanat, F., Baine, I., Kojic, E.M., Stoever, J., Liu, S., Jurczyszak, D., Bermudez-Gonzalez, M., Simon, V., Krammer, F., Zolla-Pazner, S., 2020. A High Through-Put Assay for Circulating Antibodies Directed against the S Protein of Severe Acute Respiratory Syndrome Corona Virus 2. medRxiv 2020.2004.2014.20059501.

Whitworth, C., Mu, Y., Houston, H., Martinez-Smith, M., Noble-Wang, J., Coulliette-Salmond, A., Rose, L., 2020. Persistence of bacteriophage phi 6 on porous and nonporous surfaces and the potential for its use as an Ebola virus or coronavirus surrogate. Appl. Environ. Microbiol. 86 (17), e01482-20.

Woo, P.C.Y., Lau, S.K.P., Wong, B.H.L., Tsoi, H.-.W., Fung, A.M.Y., Kao, R.Y.T., Chan, K.-.H., Peiris, J.S.M., Yuen, K.-.Y., 2005. Differential sensitivities of severe acute respiratory syndrome (SARS) coronavirus spike polypeptide enzyme-linked immunosorbent assay (ELISA) and SARS coronavirus nucleocapsid protein ELISA for serodiagnosis of SARS coronavirus pneumonia. J. Clin. Microbiol. 43 (7), 3054–3058.

Wood, J.P., Richter, W., Sunderman, M., Calfee, M.W., Serre, S., Mickelsen, L., 2020. Evaluating the environmental persistence and inactivation of MS2 Bacteriophage and the presumed ebola virus surrogate Phi6 using low concentration hydrogen peroxide vapor. Environ. Sci. Technol. 54 (6), 3581–3590.

Wu, J., Liu, J., Zhao, X., Liu, C., Wang, W., Wang, D., Xu, W., Zhang, C., Yu, J., Jiang, B., Cao, H., Li, L., 2020. Clinical characteristics of imported cases of COVID-19 in Jiangsu Province: a multicenter descriptive study. Clin. Infect. Dis. ciaa199.

Zavaleta, C., Smith, B., Walton, I.D., Doering, W.E., Davis, G., Shojaei, B., Natan, M.J., Gambhir, S.S., 2009. Multiplexed imaging of surface enhanced Raman scattering nanotags in living mice using noninvasive Raman spectroscopy. In: Proceedings of the National Academy of Sciences of the United States of America, 106, pp. 13511–13516.

Zhang, D., Ling, H., Huang, X., Li, J., Li, W., Yi, C., Zhang, T., Jiang, Y., He, Y., Deng, S., Zhang, X., Liu, Y., Li, G., Qu, J., 2020a. Potential spreading risks and disinfection challenges of medical wastewater by the presence of Severe Acute Respiratory Syndrome Coronavirus 2 (SARS-CoV-2) viral RNA in septic tanks of fangcang hospital. Sci. Total Environ. 741, 140445.

Zhang, D., Yang, Y., Li, M., Lu, Y., Liu, Y., Jiang, J., Liu, R., Liu, J., Huang, X., Li, G., Qu, J., 2021. Ecological barrier deterioration driven by human activities poses fatal threats to public health due to emerging infectious diseases. Engineering doi:10.1016/j.eng.2020.1011.1002.

Zhang, H., Harpster, M.H., Park, H.J., Johnson, P.A., Wilson, W.C., 2011. Surface-enhanced Raman scattering detection of DNA derived from the West Nile virus genome using magnetic capture of Raman-active gold nanoparticles. Anal. Chem. 83 (1), 254–260.

Zhang, J., Wang, S., Xue, Y., 2020b. Fecal specimen diagnosis 2019 novel coronavirus–infected pneumonia. J. Med. Virol. doi:10.1002/jmv.25742.

Zhao, Y., Zhao, Z., Wang, Y., Zhou, Y., Ma, Y., Zuo, W., 2020. Single-Cell RNA Expression Profiling of ACE2, the Receptor of SARS-CoV-2, 5th, 202. American Journal of Respiratory and Critical Care Medicine, pp. 756–759 2020.2001.2026.919985.